Corrosion detection and evolution monitoring in Reinforced Concrete Structures by the use of Fiber Bragg Grating sensor

S. Ali-Alvarez [*a,b], P. Ferdinand[a], S. Magne[a], and R.P. Nogueira[b]
[a] CEA,LIST, DCSI, Laboratoire de Mesures Optiques, CEA Saclay 91191 Gif-sur-Yvette, France
[b] LEPMI UMR 5279 CNRS - Grenoble INP - Univ. Savoie - Univ. Joseph Fourier, 38402 St Martin d'Hères, France

* shamyr.ali-alvarez@cea.fr; phone +33 1 69 08 99 48, fax +33 1 69 08 89 65; http://www-list.cea.fr

ABSTRACT

Corrosion of reinforced bar (rebar) in concrete structures represents a major issue in civil engineering works, being its detection and evolution a challenge for the applied research. In this work, we present a new methodology to corrosion detection in reinforced concrete structures, by combining Fiber Bragg Grating (FBG) sensors with the electrochemical and physical properties of rebar in a simplified assembly. Tests in electrolytic solutions and concrete were performed for pitting and general corrosion. The proposed Structural Health Monitoring (SHM) methodology constitutes a direct corrosion measurement potentially useful to implement or improve Condition-Based Maintenance (CBM) program for civil engineering concrete structures.

Keywords: corrosion, Reinforced concrete, Rebar, Optical fiber, Fiber Bragg Grating (FBG), Structural Health Monitoring (SHM), Condition-Based Maintenance (CBM)

1. INTRODUCTION

Corrosion of the steel bars in reinforced concrete (rebar) impacts negatively the integrity of civil facilities, making it unsafe and dangerous for users. In spite of recent developments and trends as the use of cathodic protection [1,2] or stainless steel rebar reinforcement [3-5], yet much effort remains to be done to survey the onset of corrosion processes in a reliable way. Structures owners and operators use commonly Condition-based maintenance (CBM) to determine the moment when the structure requires an intervention. The indicators employed to determine the right time for maintenance play an important role on this issue; most of them are obtained from destructives essays like concrete sampling for electrochemical analyses [6,7], others involve an indirect measurement of corrosion, like impedance or ultrasonic measures [8, 9], and all of them are punctual in space and time [10], leading to difficult parameters analyses to make the correct decision. Most of the wide used monitoring devices do not detect corrosion directly and have large ranges of uncertainty.

In terms of mechanical changes in the Rebar surface, corrosion attack depends on several chemicals and electrochemical parameters (pH, carbonation, presence of NaCl, etc.), but can mainly appear in two forms. In the first case, the metal ions oxidize and form rust that increases the internal pressure yielding to the structure crack. In another typical scenario, ions are evacuated out of the structure, with no impact in the internal strain [11]. We propose a new optical device to detect both kinds of corrosion evolution. It is based upon a pre-strained Fiber optics Bragg Grating (FBG). Fiber optics is immune to electromagnetic waves, smalls in size (125 um), low cost (mass production for telecommunication industry) and can be used simultaneously to measure different points in long distances (km). The solution involves the uses of FBG as a fuse type sensor, taking advantage of its capability of measuring longitudinal and radial strains.

2. SENSOR CONCEPTION

The Fiber Bragg Grating (FBG) is a structure formed by a periodic modulation of the refractive index in the core of an optical fiber, that acts as a reflector for a specific wavelength (λ_b), as is shown in the equation (1).

$$\lambda_b = 2 \cdot n_{eff} \cdot \Lambda \tag{1}$$

Where n_{eff} is the refractive index and Λ is the physical period of the modulation.

Physical constraints applied to an FBG can modify its periodicity, and as a consequence, its central wavelength or spectrum. These relationships are described in the equation (2).

$$\frac{\Delta\lambda_b}{\lambda_b} = \left(\frac{1}{\Lambda}\frac{d\Lambda}{dT} + \frac{1}{n_{eff}}\frac{dn_{eff}}{dT} \right)\Delta T + \left(1 - p_e\right)\varepsilon_z - (1-2\nu)\Delta P \tag{2}$$

where $\Delta\lambda_b$ is the variation of the FBG central wavelength, ΔT and the temperature variation, p_e and ν the photo elastic constant and Poisson coefficient of the silica, ε_Z the longitudinal strain and ΔP the pressure differential.

We propose to use the combination of the FBG properties previously mentioned in order to fabricate a fuse type corrosion sensor. The sensor diagram is shown in figure 1. The basic idea is that if a FBG is placed over a carbon steel plate, and then heated, besides the thermal dilatation of the iron there is a positive displacement of the FBG wavelength (first term on the equation 2). At this stage, a thin film of epoxy is applied to make both the FBG and the steel surface mutually cohesive. When the whole assembly is taken back to room temperature, the compressive strain related to the iron contraction is hence transferred to the sensor so as the FBG wavelength decreases (second term on the equation 2) under its nominal value.

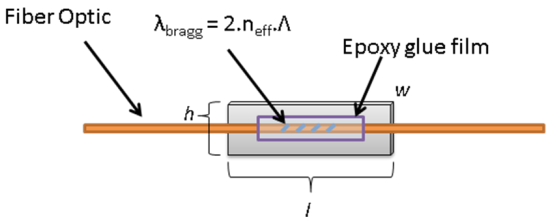

Figure 1 – Schematic representation of the FBG sensor assembly

The assembled sensor is hence ready to be submitted to different corrosion tests. Depending on the type of corrosion and the consequent accumulation or release of corrosion products, or in other words, the swallow or harvest of the metallic surface, the mechanical constraints applied to the FBG will be increased or released and the FBG wavelength is expected to consistently respond to these mechanical solicitations. An ensemble of different tests has been then carried out and the results are discussed later on.

3. EXPERIMENTAL SETUP

The sample was prepared from a mild carbon steel plate (2x1x0.6 cm^3). The corrosion FBG sensor was mounted upon a 2x0.4 cm^2 surface. All sides of the metallic plate but the FBG region were coated by a silicone film so as to confine corrosion processes to the region sensed by the probe. The sensor was pre-strained thanks to following the assembly procedure. The plate was first heat to 95 °C inducing the metal dilatation. In order to allow the sensor response to behave as explained before, the FBG was glued to the metallic surface with a high temperature polymerization epoxy resin. When the heat source was turned-off, the FBG retracted with the metallic surface being hence compressed due to the glue action that kept the contact surface solidary as predicted by equation 1. This pre-strained condition was used as a calibration start point.

A first experiment was carried out in order to validate the release theory of the pre-strain in the FBG-Corrosion probe. The test was performed in free corrosion conditions, i.e., in a liquid electrolyte NaCl (35 g L^{-1}) to allow corrosion products to freely diffuse and not to be trapped against the probe. A fast corrosion process was induced to the sample by means of a 70 mA cm^{-2} impressed current density.

Conversely, a second set of experiments was carried out in confined conditions, i.e., in a cement paste block of 6x6x7 cm^3, in order to recreate actual conditions in which corrosion products are prone to accumulate at the metal cement interface. The sensor was placed in the middle of the block, which was prepared with Portland Type 1 cement in a 0.6 proportion regarding a chloride rich water (35g L^{-1}) so as to favor corrosion initiation. After 24 hours of drying in the capsule, the resulting block was immersed in a NaOH 0,1 M + NaCl 35 g L^{-1} solution during 6 days for curing at open circuit conditions, which means without external imposed polarization. The next step was to force corrosion to take place by imposing a 100 uA cm^{-2} current density until crack, which took place after 14 days of exposure.

The FBG employed were fabricated in standard polyimide SMF. The optical measurements were made with a Burleigh WA-7600 wave meter and the electrochemical measurements with a PGZ-100 potentiometer.

4. RESULTS AND DISCUSSION

4.1. Free corrosion conditions: releasing the compressive pre-strain

In this experiment the assembled FBG plate sample was immersed in a liquid aggressive electrolyte (35 g L^{-1} NaCl solution) and polarized at 70 mA cm^{-2} to induce fast corrosion. In these conditions the corrosion products released at the interface could freely diffuse towards the electrolyte bulk so that no supplementary compressive forces were applied to the FBG. On the contrary, the fast corrosion induced by the polarization harvested the metal beneath the sample (the rest of the surface being insulated) so that the FBG and the plate disunite and the pre-applied strain was released. As explained before and as predicted from Equation 1, the main peak wavelength (MPW), was hence expected to increase. Figure 2 illustrates this issue starting from the nominal distressed FBG main peak (step 1). At high temperature just after the epoxy application, the dilated condition induces a tensile strain that increased the MPW (2). Once back to room temperature, the MPW shifts to smaller values due to retraction compressive forces (3). After the polarization with the consequent corrosion induced mass loss beneath the sensor and hence the concomitant mechanical support loss, the MPW monotonic and continuously shifted to higher values (4,6) till retrieving the starting nominal value (7). It is worth noticing that experimental values are in very good agreement with theoretical values predicted from Eq. (1) for nominal distressed, heated and retracted conditions (steps 1, 2, 3 and 7) as indicated in Table 1. The overall spectra for each case are shown in the inset. It can be seen that besides the main peak, secondary lobs appeared owing to non-ideal mechanical load or unload against the FBG surface.

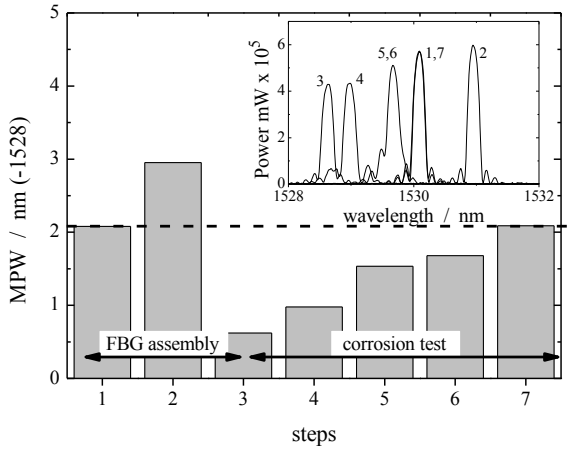

Figure 2 – Main peak wavelength (shifted of 1528 nm for the sake of label readability) at different steps of the experiment: Rest condition before sample assembly (step 1); after heating at 95 °C (2); room temperature, after sample contraction and impressed current triggered on (3), successive measurements during corrosion evolution (4 to 6), end of the test (7). Dashed horizontal line indicates the excellent retrieve of the starting value after the test. Solid points account for the theoretical predictions from Eq. (1). In the inset, ensemble of spectra measured during the experiment.

Table 1 FBG main peak wavelength calculations for the liquid electrolyte test for steps 1, 2, 3 and 7 compared to the experimental measured values

	FBG MPW		
Sensor State	Theory (nm)	measure (nm)	Error Temperature (°C)
T_0=25°C (st. 1)	1530.086		-
T_P=95°C (st. 2)	1530.933	1530.959	2.20
T_F=25°C (st. 3)	1528.669	1528.650	1.58
T_C=25°C (st. 7)	1530.086	1530.093	0.60

4.2. Confined corrosion conditions: superimposing compressive forces

The aim of this experiment was to verify the opposite behavior of the sensor regarding results presented in 4.1. By forcing corrosion processes to take place at the interface but in a mortar solid electrolyte that confined the corrosion products to the vicinity of the FBG surface, the swallowing corrosion products clusters would be expected to increase the compressive strains against the FBG surface and hence induce a decreasing tendency in the MPW evolution. Figure 3 shows that, unlikely to the monotonic evolution indicated in steps 4-7 of Figure 2 in the case of a free diffusing liquid electrolyte, in confining conditions the MPW evolution presented a noisy pattern. This fluctuating trend is certainly due to the random formation and distribution of rust clusters at the metal cement paste interface that unevenly exerted compressive strains to the FBG in the first days of polarization. As the polarization time increased, generalized corrosion became more and more intense and the strong accumulation of rust induced, as expected, a general tendency of MPW decrease after 4 days. The MPW collapse held till the FBG was broken, which happened after one week. The test went on till the sample fractured by the increasing internal forces due to corrosion products accumulation as seen in Figure 4.

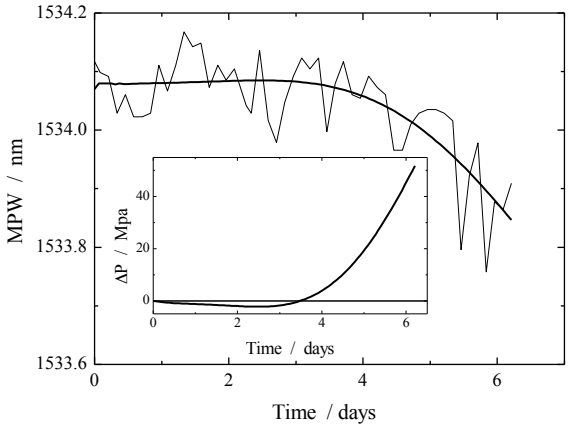

Figure 3 - Main peak wavelength evolution under 100 μa cm^{-2} imposed current density. The signal was lost during the 7th day of polarization due to the FBG rupture. Solid line: polynomial fitting. In the inset: Internal pressure variation estimated from the polynomial fitting estimated as $\Delta\lambda_b/\lambda_b = -c\Delta P$, $c = 2.87\ 10^{-6}\,MPa$.

The sample fracture was the results of expanding forces created by the swallow of corrosion products inside the concrete. As this material has a poor mechanical resistance to tractive strains, it did not support the high strain level associated. The evolution of the MPW effectively allowed the estimation of the internal forces exerting in the FBG - cement paste interface. Figure 3 shows the polynomial fitting of the noisy trend of the MPW evolution that, thanks to the simplified relationship between the MPW and DP, $\Delta\lambda_b/\lambda_b = -c\Delta P$ where $c = 2.87\ 10^{-6}\,MPa$ [12,13], the pressure gradient

could be estimated and is given in the inset of Fig. 3. It can be seen that very high expansion forces are applied to the bulk of the concrete, which can easily lead to its rupture. This value is high in comparison with the standard tensile strength of concrete (~ 3 - 5 MPa), which indicates an amplification of FBG response. It is also interesting to notice that during the first days the pressure decreased probably related to the initial metal loss that locally released the FBG support before the accumulation of corrosion products became predominant, which happened by the 4th day.

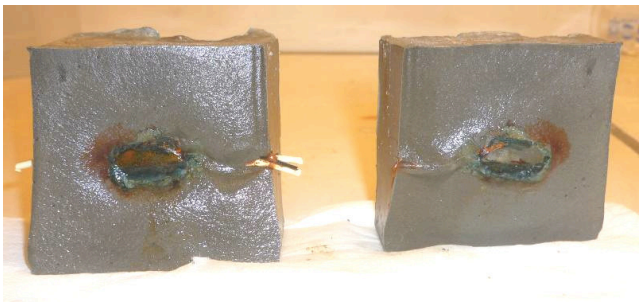

Figure 4 – Fracture of the cement paste sample due to internal strains caused by accumulation of corrosion products

4.3. Randomly distributed corrosion processes: a more complex scenario

In the two sets of experiments presented above, the interface was forced to corrode in well-controlled conditions under imposed polarization. In actual service conditions, however, corrosion is always randomly (time and space) distributed and take place at different rates so that one can expect different scenarios, as regions showing local release of corrosion products that do not accumulate (case 4.1) and other regions in which rust induced strong compressive forces are prone to appear (case 4.2). Also the formed corrosion clusters can swallow or collapse inducing compressive or tensile load variations. Consequently, the MPW long-term behavior cannot be anticipated as in the experiments discussed above.

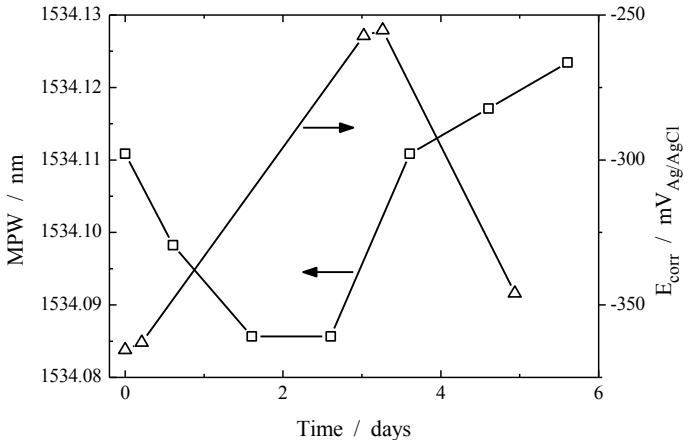

Figure 5 – Main peak wavelength (open squares) and corrosion potential (open triangles) evolution during the 6 day cure of the cement paste sample prepared from a 0.6 proportion regarding chloride rich water (35g L^{-1})

A first attempt to deal with such a complex scenario was made by following the spectra behavior during the cure of an aggressive chloride rich cement paste sample instrumented with the FBG sensor. Figure 5 shows the simultaneous evolution of the MPW and the open circuit or corrosion potential, E_{corr}. The increase of the potential during the first days of cure can be reasonably ascribed to the passive oxide film formation. On the contrary, the steep decay after 4 days is probably related to the onset of corrosion processes, which were expected due to the presence of chloride ions added to the water to favor corrosion. Indeed, according to well-established normalized values (ref ASTM 876), potential values decreasing below ca -250 $mV_{Ag/AgCl}$ indicate a probability of more than 90% of corrosion processes to take place. This probable scenario of sample corrosion is however not straightforwardly sensed by the MPW that shows a non-monotonic evolution during the cement paste cure as seen in the figure 5. As mentioned before, this must be ascribed to a complex

feature related to the solidification and hardening of the mortar with blocking pores and hardly changing conditions. The MPW should hence respond to randomly alternating tensile and/or compressive local loads related to the collapse or swallow of rust clusters that preclude it to straightforwardly follow the corrosion evolution as in the previous cases.

In spite of this apparent drawback, a sharper analysis of the overall spectra does bring information about corrosion processes evolution. Figure 6 shows, beside the main peak, an asymmetric distribution of secondary lobs at higher wavelengths. This spectra behavior is in accordance with theoretical predictions of lob appearance associated to local differences in the applied stress in FBG's, which produces a chirp in the spectral signal [14]. More interesting, these lobs show to monotonically evolve with time and hence, with corrosion in these non-controlled conditions as clearly see in the inset.

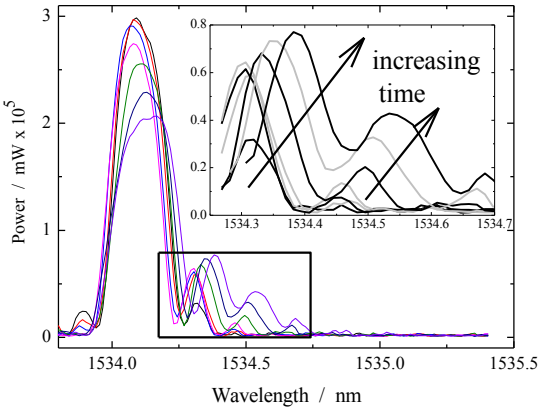

Figure 6 – Overall behavior of the measured spectra evolution during the 6 day cure of the cement paste sample prepared from a 0.6 proportion regarding chloride rich water (35g L^{-1}). In the inset: zoom of the encircled zone

It is important to stress that the monitoring of these secondary lobs is certainly difficult to explore in real service conditions. It must however be considered that this is a first set of results that seems to open up the way to the development of a new type of real-time sensor of embedded reinforcing bars in concrete structures.

5. CONCLUSIONS

In this paper we explored the possibility of use the FBG to directly measure the corrosion development in a concrete structure. The direct transduction of the iron changes to a high sensitivity fiber optic sensor increases the reliability of the measure, leading to an opportune intervention for maintenance. The two main ways of corrosion development can be detected by analyzing the spectral behavior. The dilution and diffusion of the metal ions leads to a release of the mechanical constraints, increasing the FBG central wavelength. In the other hand, the confinement of the corrosion products increase of the internal pressure progressively, and hence the mechanical constrains, decreasing the FBG central wavelength. The advantage of this system is that independently of the type of corrosion (carbonatation, presence of Cl, pitting, sulfates, microbial), their consequences over the steel can be detected and an intervention for correction can be made. However due the complexity of the corrosion development behavior, it is difficult to generalize the rules. Secondary lobes in the FBG spectrum indicate a chirping, that are caused by the random distribution of the corrosion in the steel. Further essays and modeling of the experience are required to analyze the complex scenario.

REFERENCES

[1] Christodoulou, C., Glass, G. K., Webb, J., Austin, S. and Goodier, C., "Assessing the long term benefits of Impressed Current Cathodic Protection", Corr. Sci. 52(8), 2671-2679 (2010).

[2] García, J., Almeraya, F., Barrios, C., Gaona, C., Núñez, R., López, I., Rodríguez, M., Martínez-Villafañe, A. and Bastidas, J., "Effect of cathodic protection on steel-concrete bond strength using ion migration measurements", Cem. Concr. Compos., 34(2), 242-247 (2012).

[3] Gedge, G., "Structural uses of stainless steel - buildings and civil engineering", J. Construc, Steel Res., 64(2), 1194-1198 (2008).

[4] Zhang, L., Zhang, W., Jiang, Y., Deng, B., Sun, D. and Li, J., "Influence of annealing treatment on the corrosion resistance of lean duplex stainless steel 2101", Electrochim. Acta, 54(23), 5387-5392 (2009).

[5] Mesquita, T. J., Chauveau, E., Mantel, M., Kinsman, N. and Nogueira, R. P., "Anomalous corrosion resistance behavior of Mo-containing SS in alkaline media: The role of microstructure", Mat. Chem. Phys., 126(3), 602-606 (2011).

[6] Jing, X. and Wu, Y., "Electrochemical studies on the performance of conductive overlay material in cathodic protection of reinforced concrete", Constr. Build. Mater., 25(5), 2655-2662 (2011).

[7] Martínez, I. and Andrade, C., "Application of EIS to cathodically protected steel: Tests in sodium chloride solution and in chloride contaminated concrete", Corros. Sci., 50(10), 2948 -2958 (2008).

[8] Matsumura, T., Kanazu, T. and Nishiuchi, T. "Application of Detection Technique of Reinforcing Steel Corrosion in Concrete Using AC Impedance Method to Specimens Exposed at Seashores for Seven Years", JSMSJ Japan, 51, 581-586 (2002)

[9] Miller, T., Hauser, C. J. and Kundu, T., "Nondestructive Inspection of Corrosion and Delamination at the Concrete-Steel Reinforcement Interface", Proc ASME Conference 36495, 121-128 (2002).

[10] Song, H.-W. and Saraswathy, V., "Corrosion Monitoring of Reinforced Concrete Structures - A Review", Int. J. Electrochem. Sci., 2, 1-28 (2007).

[11] Raupach, M., "Chloride-induced macrocell corrosion of steel in concrete-theoretical background and practical consequences", Constr. Build. Mater., 10(5), 329-338 (1996).

[12] Hocker, G. B., "Fiber-optic sensing of pressure and temperature", Appl. Opt., 18(9), 1445-1448 (1979).

[13] Hill, K. and Meltz, G., "Fiber Bragg grating technology fundamentals and overview", J. Lightwave Technol., 15(8), 1263-1276 (1997)

[14] Erdogan, T., "Fiber grating spectra" J. Lightwave Technol., 15(8), 1277 -1294 (1997).